Site-specific ground motion modeling for a historical Cairo site as a step towards computation of seismic input at cultural heritage sites

Hany M. Hassan[a,b,c,*], Marco Fasan[d], Mohamed A. Sayed[e], Fabio Romanelli[a], Mohamed N. ElGabry[b,c], Franco Vaccari[a,b], Ayman Hamed[f]

[a] Department of Mathematics and Geosciences, University of Trieste, Italy
[b] National Research Institute of Astronomy and Geophysics, 11421 Helwan, Cairo, Egypt
[c] North Africa Group for Earthquakes and Tsunami Studies (NAGET), Net40/OEA ICTP, Italy
[d] Department of Engineering and Architecture, University of Trieste, Italy
[e] Department of Civil Engineering, University of Toronto, Canada
[f] Faculty of Petroleum and Mining Engineering, Suez University, Egypt.

ARTICLE INFO

Keywords:
Ground motion modeling
Seismic input
Site response analysis
Cultural heritage buildings
Historical Cairo

ABSTRACT

Throughout time, the area of historical Cairo has been affected by several earthquakes from near and distant seismogenic zones. The maximum earthquake intensity reported in Cairo is VII, on the Modified Mercalli Intensity scale, due to the 1992 Cairo earthquake (Mw = 5.9). About 212 Coptic and Islamic monuments were damaged. The spatial distribution of damage, suggests the occurrence of strong local site effects in combination with high vulnerability of the cultural heritage buildings. This study presents the application of a novel seismic hazard analysis approach at a local scale based on physics-based ground motion simulations. A site-specific multi-scenario seismic input (ground motion time histories and response spectra) is computed at a heritage building in Cairo, considering the local site effect. The seismic input is calculated in three steps: a regional scale analysis followed by a site-specific analysis and the combinations of the computed scenarios ground motion. In the regional scale analysis synthetic accelerograms are computed at the site bedrock. Then, the site-specific analysis is performed to calculate the site surface ground motions or response spectra considering the local site effect. Three earthquake scenarios have been considered, characterized by different locations, magnitudes, and fault configurations. The last step consists in the combination of the computed scenario ground motion into one single multi-scenario seismic input specific for the site of interest. This input is represented by spectral ordinates and their variability. For the engineering purpose of time history analysis, the method allows also to extract the computed site specific physics-based accelerograms, requiring no amplitude scaling nor filtering by magnitudes, distances, or site classifications, as usually done with real ground motion records.

1. Introduction

Cairo is Egypt's capital and largest city, with its metropolitan area populated by about 10 million inhabitants according to the official report of the Egyptian Agency for Public Mobilization and Statistics (CAPMAS Central Agency for Public Mobilization and Statistics Arabic Republic of Egypt, 2017). The city of Cairo is culturally complex and diverse, witnessing different historical periods since its conception. The City has both ancient and modern monuments and acts as an open museum with ancient Egyptian, Greco-Roman, Coptic, and Islamic monuments. Cairo, in its current form, dates back to the Islamic conquest of Egypt by Amr ibn al-Aas in 641 (Behrens-Abouseif, 2000). Historical Cairo is nowadays located in the eastern part of the modern metropolis, and contains the remains of Fatimid Cairo, Fustat, al-Askar, and al-Qatta'I, which were capitals before al-Qahira (Cairo). It comprises many archaeological sites such as the Hanging Church, one of the oldest churches in Egypt, the mosque of Amr ibn al-Aas, which is considered the oldest mosque in Africa, and many other residential, administrative, and public service buildings, in addition to several mosques, madrasas, hammams, and fountains registered by the United Nations Organization for Education, Science and Culture (UNESCO) as World Cultural Heritage sites.

On October 12, 1992, an earthquake of moderate size ($5.9M_w$) struck the city and produced widespread impacts on the built environment. This event lead to the death of 500 people, about 6500 were injured, and more than 8300 buildings suffered different levels of

* Corresponding author.
E-mail address: hany_hassan@nriag.sci.eg (H.M. Hassan).

damage, as reported by Sykora et al. (1993) who indicated that the damage was concentrated in the areas of greater Cairo, Nile Valley, and its Delta. The maximum observed intensity near the earthquake epicenter was about VIII on the Modified Mercalli Intensity (MMI) scale. The highest MMI rank in Historical Cairo was VII, where about 212 Coptic and Islamic monuments were damaged (Sykora et al., 1993). The spatial distribution of the damage suggests the occurrence of strong local site effects in combination with the high vulnerability of many of the existing old structures. This is evident from the different damage levels observed in historical Cairo between buildings having the same construction period and similar engineering conditions. Buildings built on weak fill soil layers encountered significantly more damage than those built on limestone bedrock. The fill layer, formed by building and rebuilding activities in Cairo through history, could pile up to a height of a few tens of meters; generally, this soft layer amplifies the propagated ground motions, leading to greater observed damage.

Many monuments of historical Cairo suffer from severe deterioration due to several factors that have detrimental impacts on their structural integrity. This causes irreparable damage, and in some cases failure of the monuments (e.g. groundwater, poor building condition, inadequate seismic resistance, and absence of maintenance, protection and preservation policies) even for modest seismic events. Thus, proper site-specific seismic hazard analysis that accounts for the parameters that influence site amplification (e.g. resonance, surface and subsurface topography, the geometry of the sedimentary layers, wave conversions) is necessary to find and select proper mitigation strategies to help in the conservation of these invaluable structures.

Few noise-based studies focused on seismic site-response in Cairo (e.g., Gamal, 2009). Noise-based methods (e.g., H/V) alone cannot adequately provide an accurate estimation of site-effects for the site of interest. El-Sayed et al. (2004) and Kebeasy and Husebye (2003) have studied with a scenario-based approach the local effects for specific sites located south of Cairo. They have concluded that the loose sediments of the Nile Valley and the Nile Delta can strongly amplify the seismic ground motion from far and near-field earthquakes. Therefore, the pre-event strong ground motion modeling in a megacity like Cairo is essential and indispensable for reducing the potential socio-economic impacts from future earthquakes.

The current study presents the application of a novel seismic hazard analysis approach at a local scale to compute multi-scenario seismic input at a cultural heritage building site in historical Cairo; ground motion time histories and related response spectra are computed taking into account source (e.g. directivity) and site effects. The geology and seismicity of Cairo are introduced along with the input data (earthquake scenarios and site profiles) required for performing the ground motion simulations. The calculated multi-scenario seismic input, in the form of time histories and response spectra at the site surface, can be used for the seismic evaluation of the heritage buildings. This study represents a base of knowledge for the seismic risk assessment of assets in historical Cairo, which deems crucial for the conservation of numerous cultural heritage buildings.

2. Geology and seismicity of Cairo

Cairo stretches along both sides of the Nile River at about 20 km south of the location where the river divides into the Rosetta and Damietta branches. The city lies entirely within the floodplain of the Nile River with a width of about 12 km from Mokattam hills on the southeast to the Pyramids plateau on the west. A number of formations that represent different geologic epochs characterize the surface geology of the city as shown in Fig. 1. For the purposes of this study, three site cross sections denoted as I (NS), II (NS), and III (EW), which are shown in Fig. 1 as blue line, are extracted to perform the analysis as will be described in later sections. The oldest rocks are exposed in Abu Roash and Pyramids plateau and belong to the Cretaceous period. The Eocene formation, composed of limestone, outcrops in the Mokattam hills in the east and Pyramids plateau in the west. The Oligocene in the area is represented by two different facies: sands and gravels of the Gebel Ahmer type and Basalt flow. The Miocene is composed of marine sediments, made up of sandy limestone and sands enriched with fossils, which has outcrops in the northeast Cairo. Finally, the Pliocene marine deposits, exposed south of the Sphinx ditch, are represented by marls and sandy limestone beds. The detailed description of the subsurface geology of Cairo city is discussed in Said (1975), Shata (1988), Said (1990) and Said (2012). The landscape areas around Cairo (east and west) are highly affected by different fault systems (EGSMA, 1981; Said, 1990). The most predominant of these systems are those of EW (Mediterranean trend) and NW - SE (Clysmic fault), which are reported on both the surface and subsurface of the Cairo area. These faults are mainly normal, with steep planes, and form a portion of a graben and horst complex (Shata, 1988). Minor folding associated with faulting is identified in Gebel Mokattam and east Heliopolis areas. In Abu Roash, the dominant geologic structure is folding, which is a part of the Syrian arc system; a system of folds crossing the unstable shelf area of northern Egypt (Shata, 1988). Said (1981) has shown that the basin, having a depth of about 2.5 km, was fault-bounded and was subsequently eroded by the Eonile in late Miocene.

The spatial distribution of earthquakes shows that seismic activity is concentrated in the northern part of Egypt, with Cairo surrounded by a number of active seismic sources, i.e. Dahshour and Cairo-Suez district sources (Mohamed et al., 2012) as shown in Fig. 2. In Fig. 2, the historical and instrumental seismicity (for events with magnitude larger than 3) is plotted and overlaid with geologic and active faults and main tectonic features; the earthquake scenarios selected in this study for the ground motion modeling are marked with green bull eye. The available data for historical earthquakes in northern Egypt date back 4000 years. The first documented earthquake is believed to have occurred around 2200 BCE (Kebeasy and Maamoun, 1981). The history of earthquakes felt in Cairo indicates that moderate or high levels of shaking occur rather infrequently.

Previous research (e.g. Ambraseys et al., 2005) shows that the location of the seismic sources, which are responsible for the damage in historical monuments, are from near and distant seismogenic sources (e.g., Dahshour seismic source, Eastern Mediterranean, and Dead Sea fault system). The damage can be attributed to any or all of these factors: continuous degradation of foundation and structural masonry from environmental effects (especially groundwater), inadequate lateral structural resistance and the subsequent imposition of light to moderate earthquake forces (Ambraseys, 2001).

Recently large earthquakes worldwide have evidenced the profound effects of site conditions on the spatial distribution of earthquake damages (e.g. September 19, 2017, 7.1Mw Puebla, Mexico earthquake). Ambraseys (2001) studied the effects of distant earthquakes (originated in Hellenic arc at epicentral distances ranging between 300 and 1200 km) on the Nile Delta and Cairo concluding that the ground motions from large earthquakes (~5.5+) of shallow to intermediate focal depth are capable of producing widespread damage in north Egypt region (e.g. Mediterranean earthquakes of February 17, 1810, 7.5M_w and September 12, 1955, 6.1M_w). On the contrary, earthquakes of similar magnitudes that occurred along the Gulf of Suez, Gulf of Aqaba, and the Red Sea Gulf (1969, Shedwan earthquake (6.9M_w) and 1995, Aqaba earthquake, (7.3M_w)) have also been felt in the north Egypt region, but occurred without significant damage. This could be because seismic waves triggered by east Mediterranean's earthquakes encounter less attenuation propagating to the south.

3. Methodology

Earthquake based seismic zonation for a specific area can be performed through empirical seismic methods, that require an extensive dataset of strong motion records from all the potential earthquake sources (weak or strong events) at the site of interest; alternatively, it

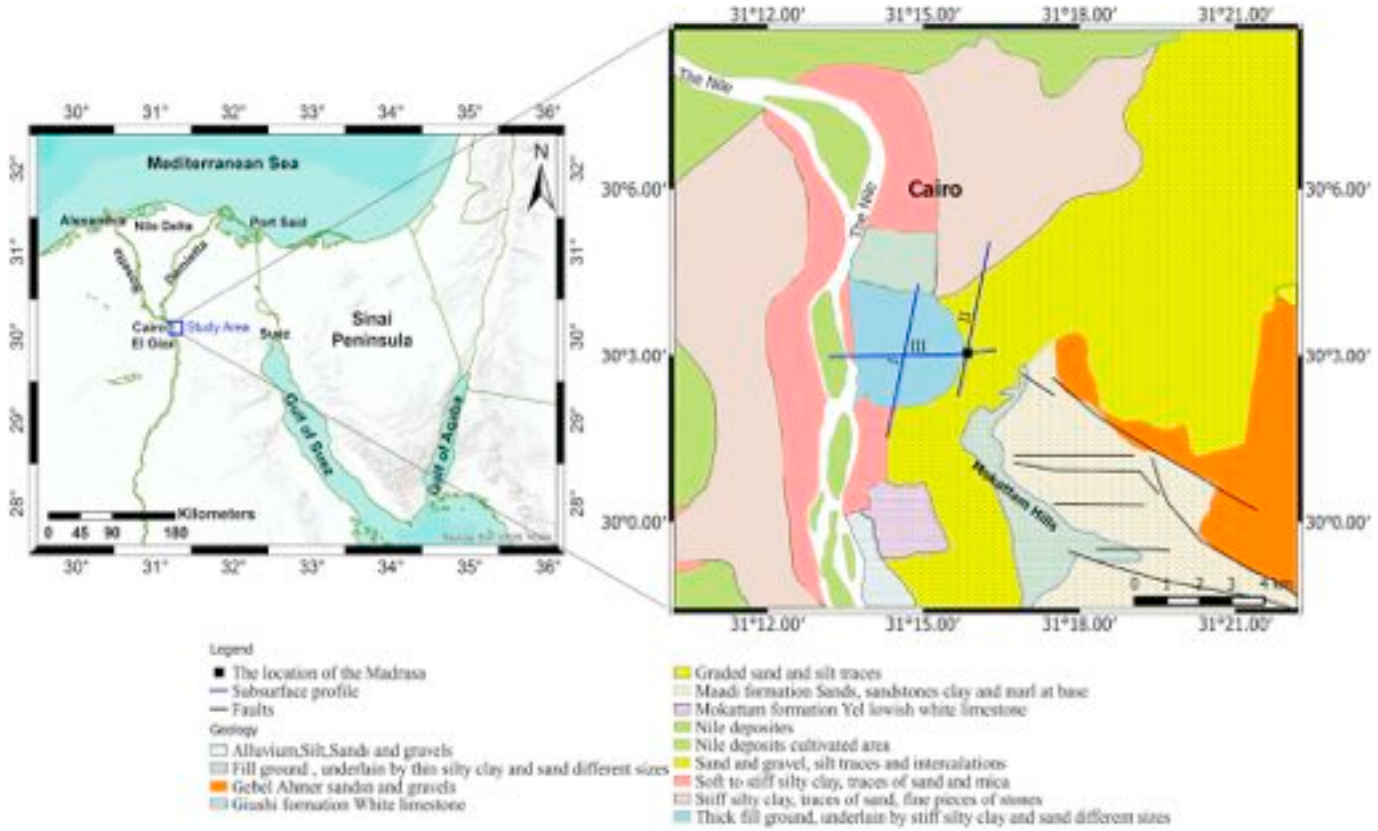

Fig. 1. Northern Egypt map (left) and zoomed surface geology map of the area of interest combined with the location of the site cross sections (right). (The site of the cultural heritage building for which the seismic input was computed is marked with a black square).

could be based on realistic modeling of the ground motion scenarios developed from the physical knowledge of seismic waves generation and propagation. In some circumstances, the use of empirical methods for a given site is not possible, due to the scarcity of ground motion data in the region. A preventive tool that makes use of realistic physics-based modeling of ground motion from postulated earthquake scenarios is represented by the Neo-Deterministic Seismic Hazard Analysis (NDSHA). This method can be used before the occurrence of strong earthquakes, thus helping reduce the risk associated with impending earthquakes (see Panza et al. 2001 and 2012; Magrin et al., 2016, and the references therein). Hassan et al. (2017) provided a set of seismic hazard maps for Egypt computed within the framework of NDSHA procedure at national scale. These maps are computed based on the modeling of the seismic waves propagation. Seismograms calculation is based on the Modal Summation (MS) technique and the sources are modeled as Size and Time Scaled Point Sources (STSPS) as proposed by Panza et al. (2001, 2012).

At local scale, further investigations can be performed in order to compute physics-based accelerograms accounting for source effects, path and local soil conditions. Such realistic synthetic time histories can be used to perform dynamic analyses of relevant structures, such as infrastructures, historic, and critical buildings.

Using multi-scenario physics-based ground motion simulations Fasan et al. (2016) and Fasan (2017) proposed a procedure to define the seismic input (e.g., response spectra and related time histories) based on a multi scenario seismic hazard analysis approach. The procedure is illustrated in Fig. 3 and the output can be adopted directly in the seismic design and assessment of buildings. Related synthetic accelerograms can also be used without carrying out any additional steps such as amplitude scaling or filtering. Applying this procedure, response spectra can be computed directly from physics-based broadband simulations of the seismic process (Fasan, 2017). According to Fasan (2017) if all possible scenarios are accounted for in the hazard analysis, this procedure can lead to an estimation of the upper bound ground motion at the site of interest called Maximum Credible Seismic Input (MCSI).

This multi-scenario seismic input is computed at the site of interest in three steps. The first analysis, called the regional scale analysis (RSA) computes the expected ground motions at the site bedrock. Computations should be performed considering all possible sources at different locations. Laterally non-varying crustal models are considered to mimic the propagation path of seismic wavefield from source to the site, thus, without considering the local site heterogeneities. The second analysis, defined as Site-Specific Analysis (SSA), taking the local site effects into account provides a site-specific seismic input at the site surface. SSA takes into account both structural and site heterogeneities by using local finite difference calculations. In SSA, the wavefield generated by the modal summation technique is introduced into a mesh that defines the local lateral heterogeneity propagation (e.g., Panza et al., 2001; El-Sayed et al., 2004).

The third step is the computation of the multi scenario response spectrum, built by selecting the most hazardous source at each vibrational period on the base of the median spectral acceleration of the simulations from every source. Uncertainties related with earthquake source parameters are accounted for by performing an initial parametric analysis and using a stochastic simulation of the rupture process varying the enucleation point, the rupture velocity and the slip distribution on the fault plane. Soil parameters are usually defined using mean properties however their variability can also be taken into account using many “realizations” of them as done for the source.

All the available surface and subsurface geological, geophysical, seismological, seismotectonic and morphostructural zonation (MZ) information for a specific site can be used to realistically generate the synthetic seismograms from all the possible seismic sources that could

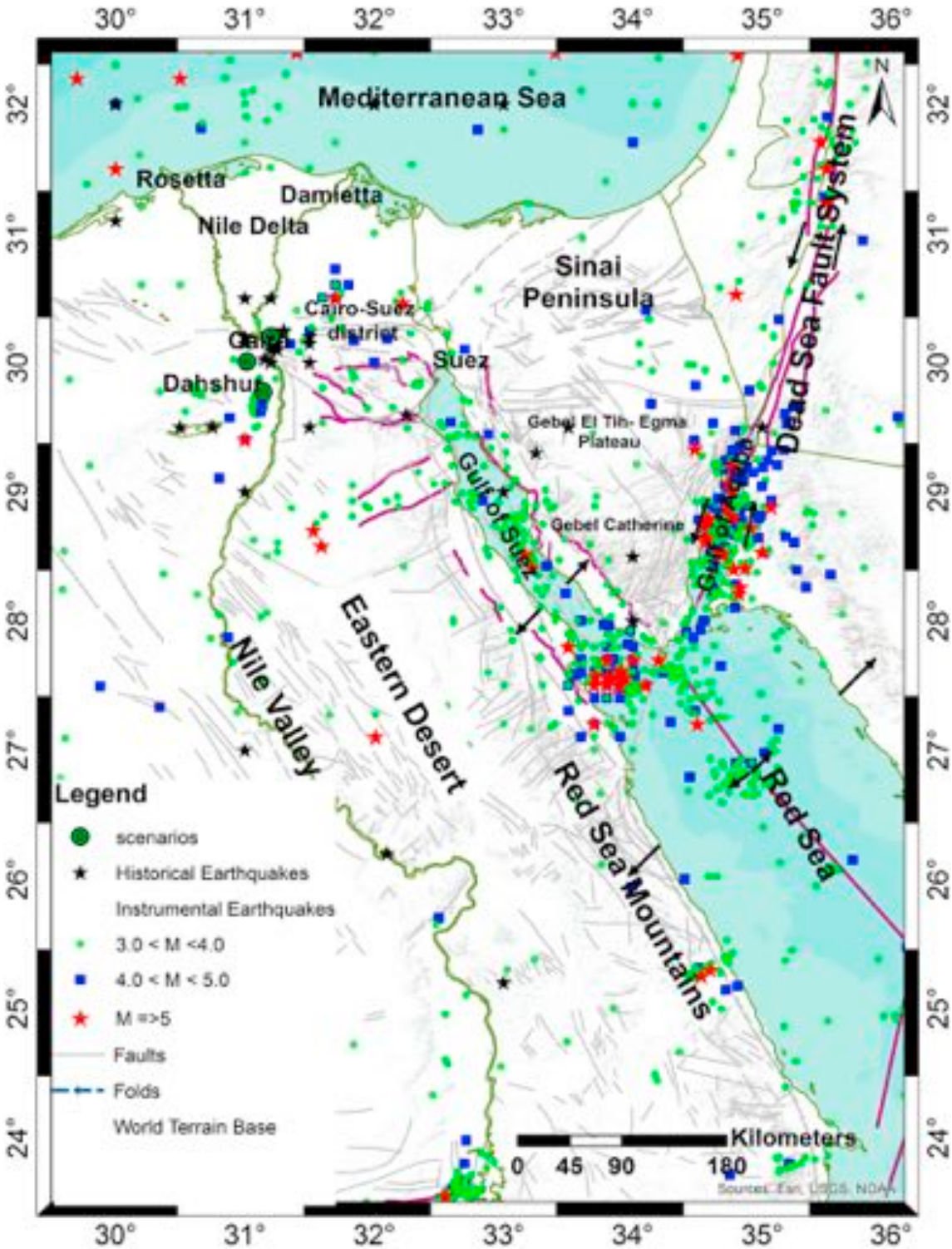

Fig. 2. Historical (black stars) and instrumental (classified into 3 classes of magnitude: 3–4, 4–5 and > 5, marked with green circles, blue squares and red stars, respectively) seismic events are displayed together with the geologic faults and main tectonic features of the northeast part of Egypt. The three earthquake scenarios adopted for the ground motion modeling in this study are marked with green bull eyes. (For interpretation of the references to colour in this figure legend, the reader is referred to the web version of this article.)

affect the site of interest (Panza et al., 2001), as illustrated by the scheme in Fig. 4.

A hybrid technique (e.g. Fäh et al., 1993; Panza et al., 2001) that combines both modal summation (MS) and finite difference (FD) techniques (Fig. 5), is used to simulate the ground motion induced in laterally heterogeneous structural models at the site of interest. This approach has been successfully applied for the purpose of the neodeterministic seismic microzonation in several urban areas around the world, e.g. Rome (Fäh et al., 1993), Beijing (Sun et al., 1998), Naples (Nunziata et al., 2000), Delhi (Parvez et al., 2004), and Sofia (Slavov et al., 2004). The modal summation is applied to simulate wave propagation from the source to the sedimentary basin of interest. Being a

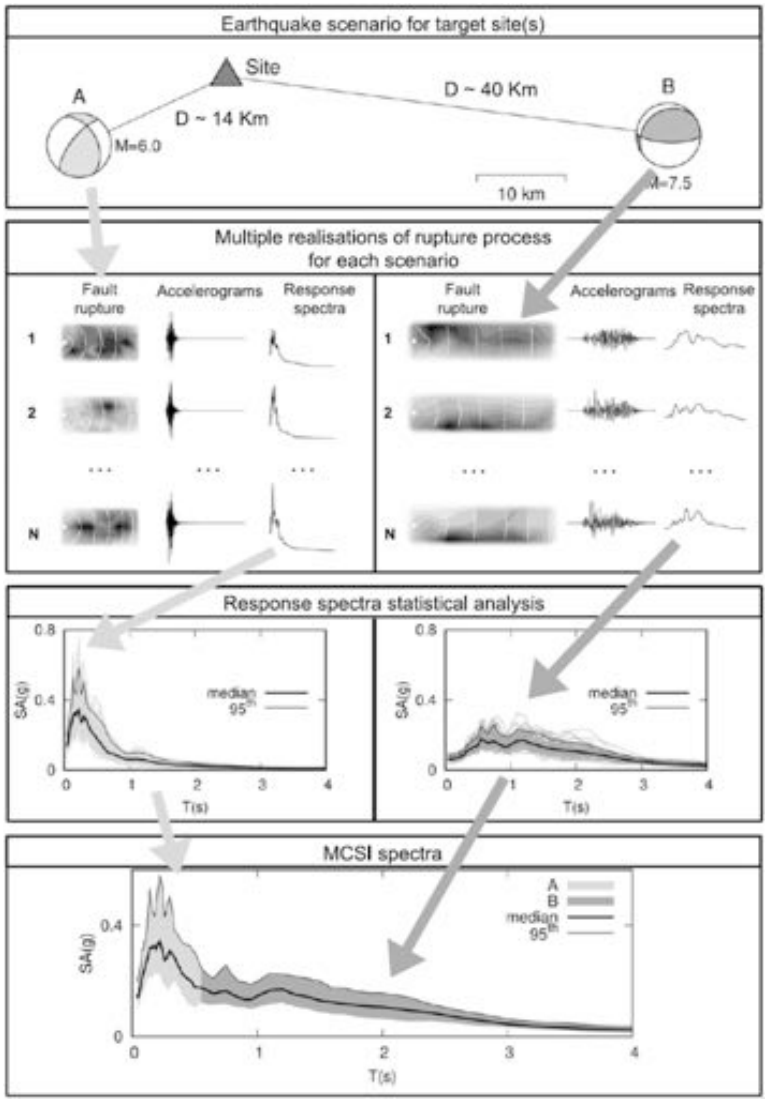

Fig. 3. Description of the multi-scenario seismic input definition procedure after Fasan (2017).

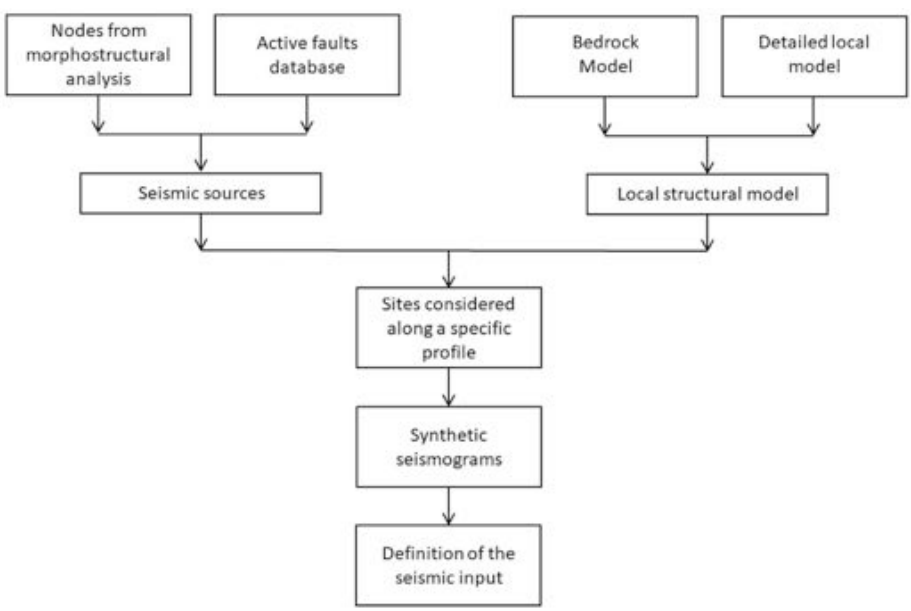

Fig. 4. Flow chart of the neodeterministic method for seismic hazard assessment at local scale.

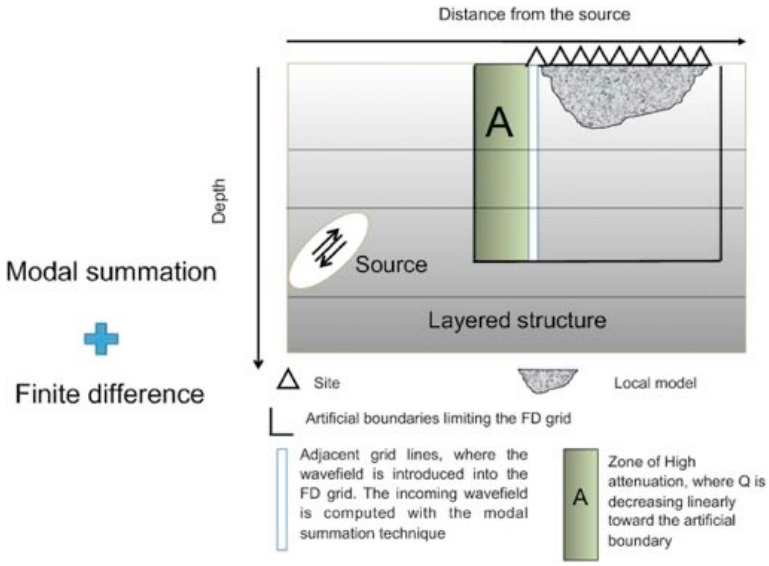

Fig. 5. Scheme of the modal summation-finite difference hybrid technique (Q is the quality factor).

pure analytical technique, there is no time penalty applied in this part of the modeling associated with the model size. Finite difference method is then applied to propagate the incoming wavefield in the laterally heterogeneous part of the structural model (Fig. 5).

Each of the two modeling methods, i.e., MS and FD, is applied in the part of the structural model where it is most efficient. The MS technique is applied to simulate wave propagation from the source to the sedimentary basin of interest (profiles or cross sections of the lateral heterogeneity). On the other hand, the FD method is applied to propagate the incoming wavefield in the laterally heterogeneous part of the structural model that contains the sedimentary basin. The travel path from the seismic source position to the local heterogeneous structure of interest is approximated by a structure composed of one-dimensional (1D) laterally homogeneous layers. The coupling of the two methods is carried out by introducing the resulting time histories obtained with the MS into the FD computations. For the application of the FD technique, the local structure is discretized into a grid mesh, whose step has to be small enough so that there are at least ten points per wavelength.

This analysis allows to evaluate amplifications or de-amplifications along the heterogeneous profile with respect to the bedrock model; the amplification patterns are obtained according to the response spectrum (RS) ratio scheme as shown in Fig. 6. At each mesh node along the cross section topography, the response spectrum of the calculated synthetic accelerogram is computed for two cases: (a) RS_{1D} for the reference bedrock 1D model assuming no lateral heterogeneity of the bedrock structural model (Fig. 6 bottom); and (b) RS_{2D} for the realistic laterally heterogeneous 2D model shown in Fig. 6 (top). Then, the response spectra ratio (RSR) = $RS_{2D\ (Laterally\ heterogeneous\ model)}/RS_{1D(Reference\ bedrock)}$ (RSR 2D/1D) at each site is calculated to provide the site bedrock amplification expected at different frequencies due to the characteristics of the local structural model. The procedure is repeated for all the mesh nodes along the profile topography. This is done in order for the general amplification pattern (increase of amplitude) to be obtained by contouring the distribution of amplification value along the profile, as a function of frequency and epicentral distance along the cross section. The site amplification in the terms of RSR has been validated in several previous studies (e.g. Panza et al., 2001, 2012; Parvez et al., 2004).

4. Site-specific ground motion modeling for Historical Cairo

The calculation of synthetic seismograms at the site is performed using the MS-FD hybrid technique in order to investigate the effect of the propagation path and localized lateral heterogeneity on the

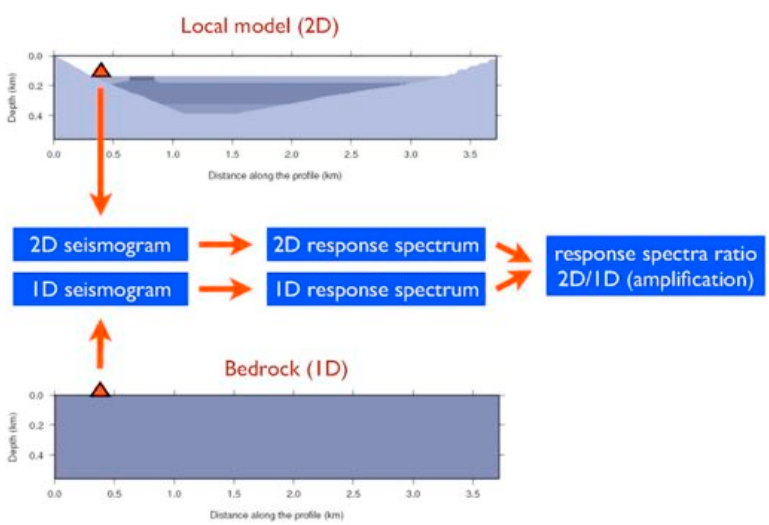

Fig. 6. Scheme for the estimation of RSR ratio at a site along a profile cross section.

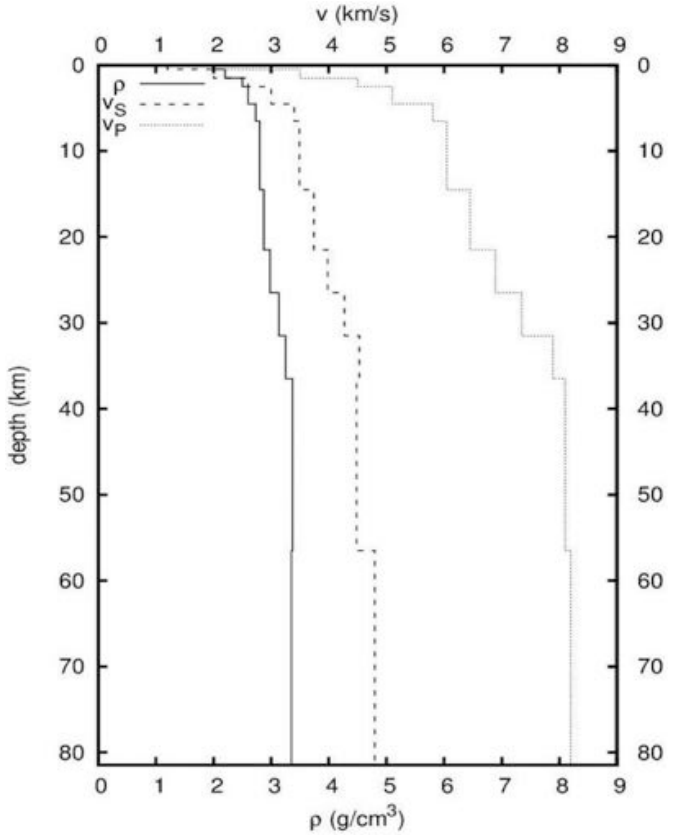

Fig. 7. Seismic velocities (V_P and V_S) and density (ρ) of the regional bedrock model.

wavefield. The seismic wavefield is computed first in a laterally non-varying structural model with the MS technique. The regional bedrock model (Fig. 7) from the study of El-Khrepy (2008) is employed in this study. The computed wavefield is then introduced in the laterally heterogeneous model composed using lithology and thickness of the borehole data published by Said (1975); their mechanical properties were estimated based on ambient noise survey.

4.1. Identification of earthquake scenarios

Parametric studies are crucial in identifying the earthquake parameters that could cause the maximum ground motion at a given site. Romanelli and Vaccari (1999) and Lokmer et al. (2002) showed that the focal mechanism of the earthquake scenario can play an important role in the modification of seismic ground motion at a given site. Sometimes it dominates the effects of the local structure. The variability in the source parameters can be tackled considering several rupture process realizations for each earthquake scenario, different focal depths, and fault orientations. Parameters extracted from the synthetic accelerograms can be calibrated against the available records, if any.

Hassan et al. (2017) performed a RSA for Egypt producing seismic hazard maps computed within the framework of NDSHA. Those maps incorporate all available information (i.e. instrumental and historical seismicity, active faults, Morphostructural Zonation (MZ) data) (Gorshkov et al., 2019) about earthquake scenarios that may affect the area of study.

From that RSA three earthquake scenarios (shown in Table 1) have been selected to compute the amplification patterns along 3 different heterogeneous sections (Fig. 1) across the historical Cairo area and the seismic input at a site of interest located at the intersection of sections II and III. The selected scenarios are those that show the highest spectral accelerations in the range of vibrational periods from 0 to 4 s. These scenarios have been found to be of magnitude 5.9–7.0 M_w earthquakes at a distance between 10 and 25 km, north and west of the site of interest. The selected scenarios comprise one instrumental and two historical events as illustrated in Table 1.

The instrumental earthquake that occurred on October 12, 1992, identified as scenario 1, is adopted as the seismic source in the modeling of NS cross sections I and II (Fig. 1). The other two nearby scenarios of interest to the historical Cairo area are labeled as scenario 2 and scenario 3. Scenario 2 is selected as a seismic source in the modeling of NS cross sections I and II, while scenario 3 is accounted for in the modeling of EW cross section III.

Hypocentral depth, magnitude, and other geometrical seismic source parameters (i.e. strike, dip, rake) are reported in Table 1. Variations in the kinematic parameters related to the rupture process on the fault plane are accounted for through multiple realizations (e.g. Gusev, 2011). In fact, the focal mechanism and rupture process of earthquake scenarios could play a crucial role in the modification of seismic ground motion at a given site, sometimes dominating the effects of the local structure itself (source-dependent amplifications). The possible variations in the seismic source rupture can be tackled considering different directivity angles, rupture styles and several rupture process realizations for each earthquake scenario, different focal depths and fault orientations. For each of these realizations synthetic seismograms are computed with 10 Hz cutoff frequency adopting a double couple, size and time scaled, point source (STSPS) representation as described in Panza et al. (2012).

4.2. Local site conditions at the site of interest

There can be significant differences in site conditions from one location to another due to variations in geological formations, thickness, properties of soil/rock layers, depth of bedrock and water table, and surface and underground topography. These variations can have significant effects on the characteristics of earthquake motions on the ground surface.

The laterally heterogeneous soil profile of the site has been composed using data from literature and fieldwork. The detailed subsurface local soil profile, incorporating the data of 217 shallow boreholes, representing the site conditions beneath most of the monuments in historical Cairo have been introduced by Said (1975). These data were used to evaluate the site-specific ground motion modeling at the site of interest. The site is composed of fill overlying silty clay underlain by thick sand and gravel layers, varying vertically and horizontally in the site of interest as shown in Fig. 8 and Fig. 15. The average depth of the soil layers in the various cross sections developed by Said (1975) is about 60 m below the mean sea level, and then they have been further extended to approximate the bedrock depth of 120 m, based on the study by Toni, 2012. The average details of the physical properties of the soil layers at the site are adopted after Toni, 2012. The quality factors (Q) for P- and S-waves for different soil types are adopted using the study of El-Sayed et al. (2004). A Pleistocene-age plastic clay layer is believed to underlie the entire alluvial valley (Said, 1975). General description for the soil column at the study area from the top is here described.

a) Fill layer:

Most of the city of Cairo is built on a layer of fill material made up of builder's rubbish or refuse heaps, either from the remains of old buildings that had decayed and/or fallen down. Canals, remnant river channels, and ponds that are found on maps from the 14th century have been filled with the aforementioned materials (Said, 1975). This layer significantly varies in thickness range between a few meters to 40 m with an average of 15 m. The shear wave velocity (Vs) for this layer is low, ranging between 170 and 270 m/s.

Table 1
Parameters of earthquakes scenarios adopted in this study compiled from the study of Hussein et al. (2013).

Scenario		Location		Magnitude	Focal depth (km)	Focal mechanism			Cross sections	Place of the Source	Epicentral distance (km)
No	Date	Lat	Lon			Strike (°)	Dip (°)	Rake (°)			
1	12 October 1992	29.74	31.63	5.8–5.9	20	285	66	−117	I (NS)	South	26
									II (NS)	South	30
2	25 July 950	30.20	31.20	6.5–7.0	10	136	42	−75	I (NS)	North	20
									II (NS)	North	15
3	April 857	30.00	31.00	6.5–7.0	14	136	75	−70	III (EW)	West	22

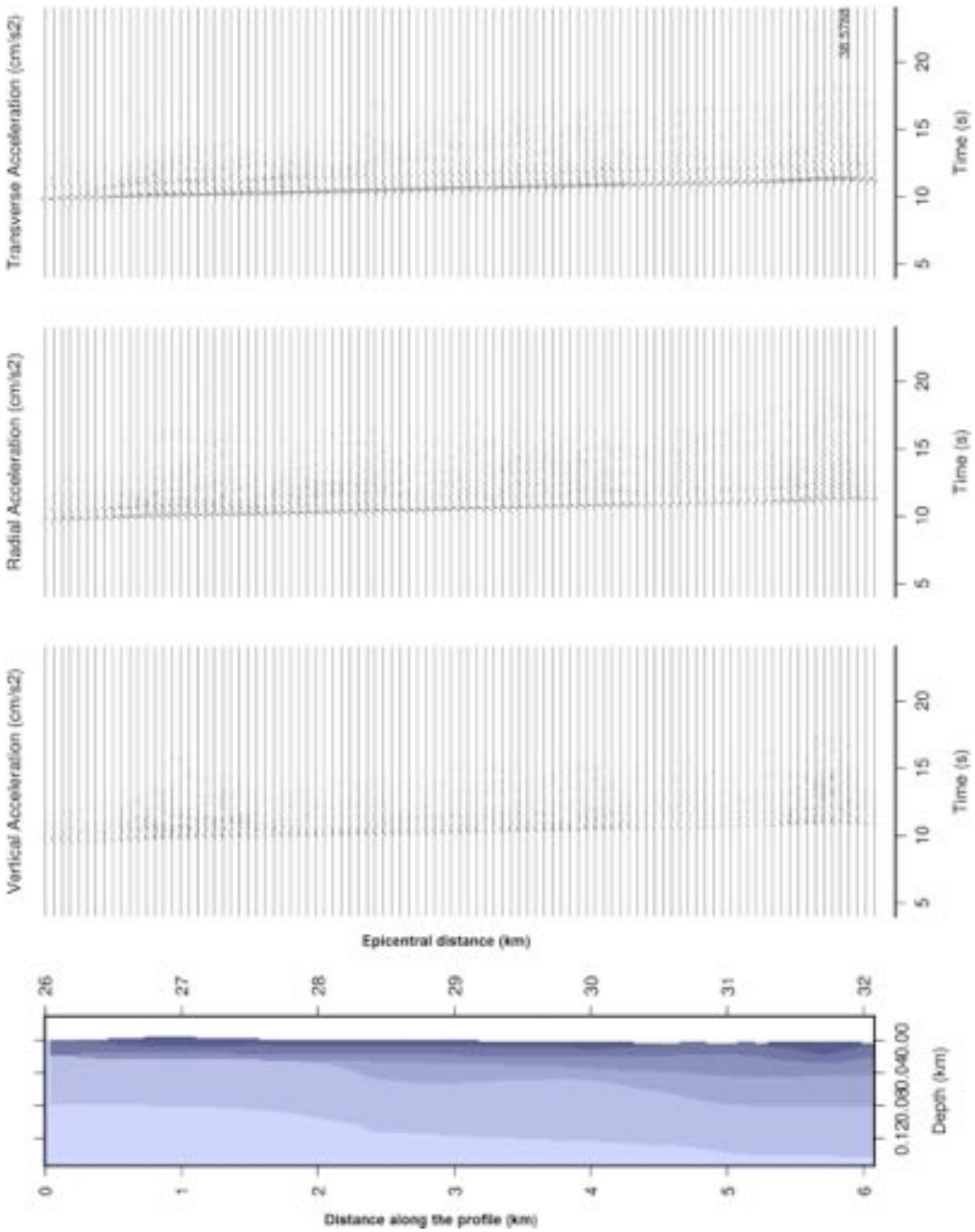

Fig. 8. Three-components synthetic accelerograms at the ground surface for scenario 1 along cross section I.

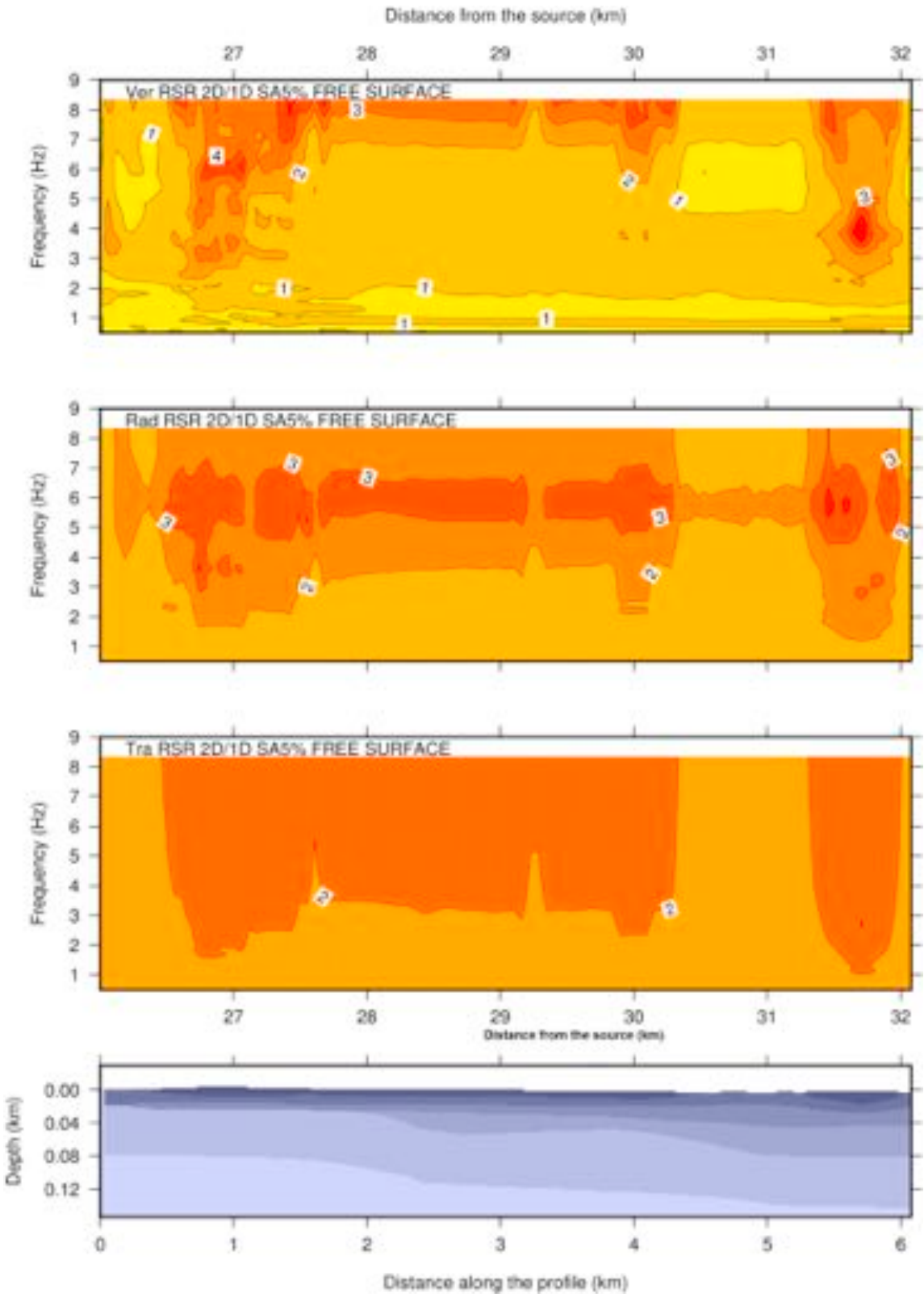

Fig. 9. Response spectra ratio (RSR 2D/1D) at 5% damping for computed three-components synthetic accelerograms for scenario 1 along the cross section I.

b) Holocene clay-silt layer:

This layer contains the modern mud of the Nile and its thickness is distributed uniformly, varies from 8 to 10 m in most of the available boreholes in the Cairo area. The mud is dark gray to brown in colour and contains clay and sandy clay (for more details see Said, 1975). The measured Vs for this layer ranges between 415 m/s to 460 m/s.

c) Pleistocene graded sand-gravel layer:

This layer has been recognized almost in all the available boreholes in the city. The content of this layer may be coincident with the exposed

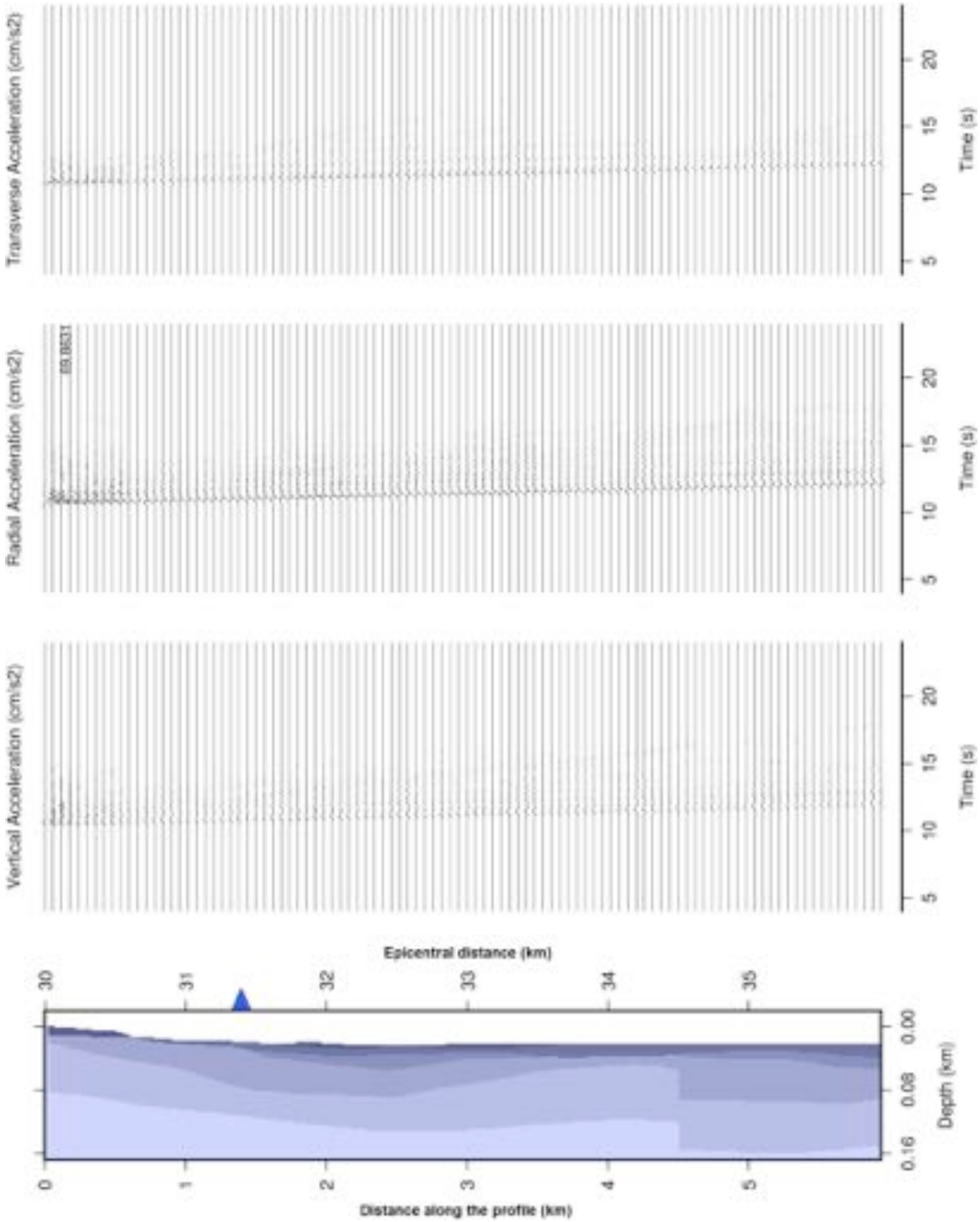

Fig. 10. Three-components synthetic accelerograms at the ground surface for scenario 1 along the cross section II.

gravel layer on both the east and west banks of the Nile River. The isopach contour map of this layer shows that the layer thickness increases northward with a maximum recorded thickness of 90 m in the Zaitun basin, while the minimum thickness has been encountered in the boreholes at the eastern side of the Nile River (Said, 1975). The layer's Vs vary between 500 and 750 m/s.

d) Plastic clay layer:

This layer is made up of two units. The upper unit consists of silts and clays while the lower unit consists of clays with brackish water micro-fossils. This layer lies at about a 100 m depth in Cairo, forming the base for the valley sediments and overlies the Oligocene gravel and sand of the Gebel Ahmar type. This layer thickness ranges from a few meters to 90 m. Plastic clays may exist at shallow depths in some locations, which could shrink and swell in volume if the groundwater fluctuated significantly. In the historical Cairo region, the plastic clay layer has a thickness varying from 20 to 40 m.

4.3. Ground motions modeling from scenarios 1 and 2 (NS cross sections I &II)

From the RSA modeling of ground motions at the bedrock (see Hassan et al., 2017) along NS cross sections I and II, the October 12,

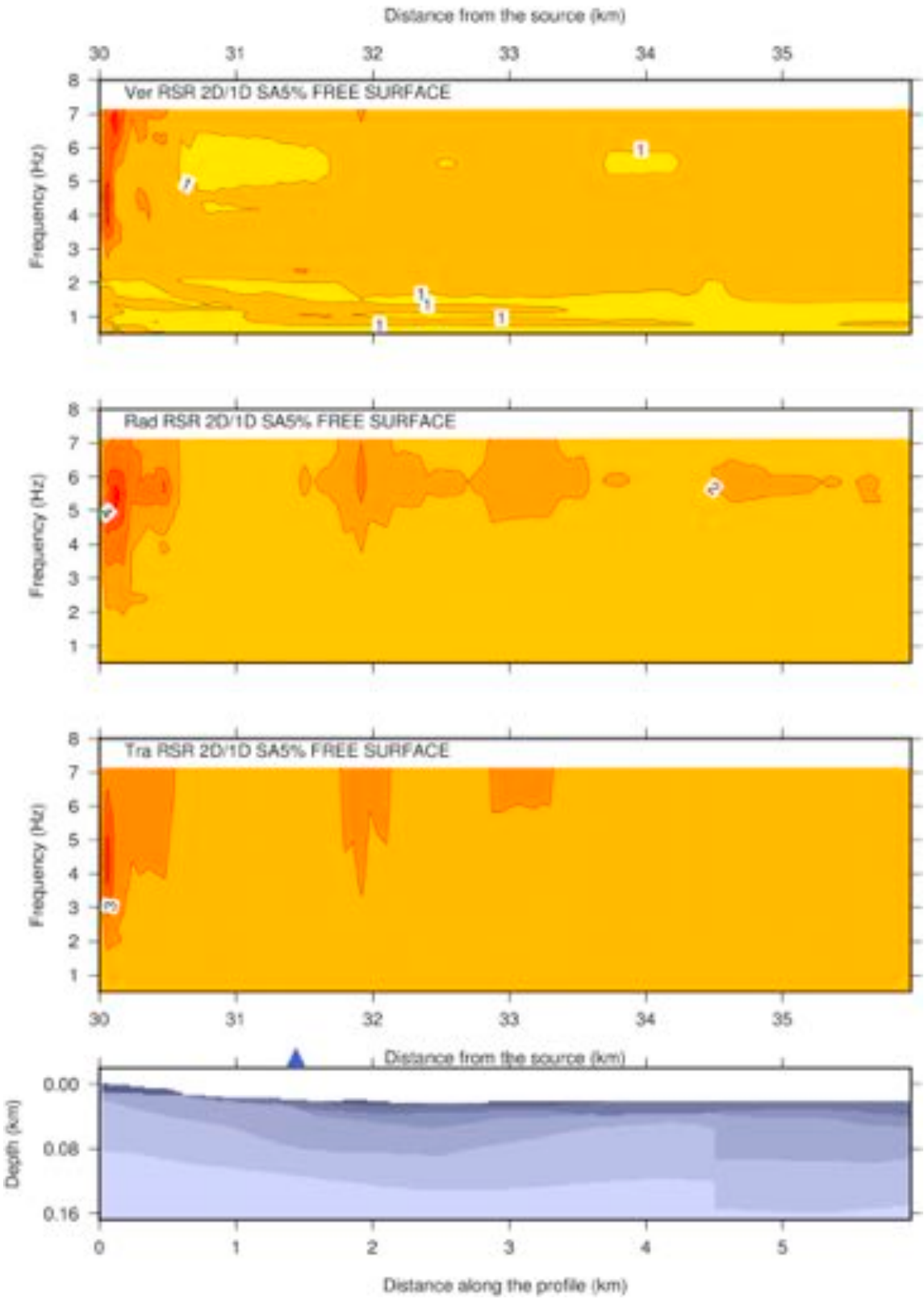

Fig. 11. Response spectra ratio (RSR 2D/1D) at 5% damping computed for three-components synthetic accelerograms for scenario 1 along the cross section II. The blue triangle marks the location of the site for which the response spectra are provided. (For interpretation of the references to colour in this figure legend, the reader is referred to the web version of this article.)

1992 earthquake as scenario 1 (MMI = VIII, 5.8–5.9 M_w) and 950 earthquake as scenario 2 (MMI = IX, 6.5–7.0 M_w) have been used (Table 1). The synthetic accelerograms are calculated with a cutoff frequency of 10 Hz using the MS-FD hybrid approach for an array of mesh grids regularly spaced at 60 m along the NS cross sections (I and II). The three components of the calculated synthetic accelerograms in transverse, radial, and vertical directions from scenario 1 along cross sections I and II are shown in Fig. 8 and Fig. 10, respectively.

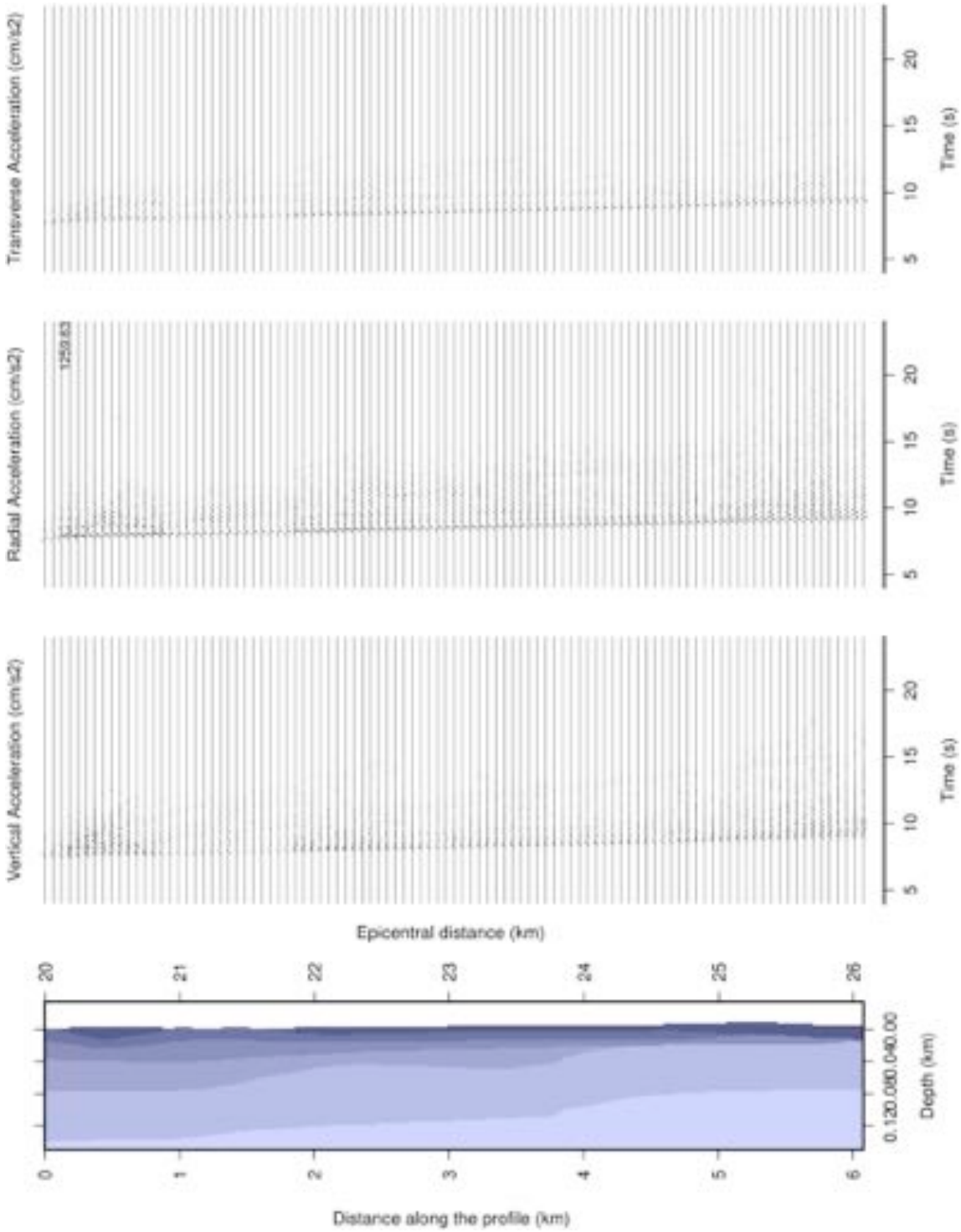

Fig. 12. Three components synthetic seismograms computed at the ground surface for scenario 2 along the cross section I.

The plots of response spectra ratio (RSR 2D/1D) from scenario 1 along cross sections I and II are shown in Figs. 9 and 11, respectively. RSR is the ratio between the response spectrum of the calculated synthetic seismograms from the lateral heterogeneous 2D model (local profile) and the response spectrum of the calculated synthetic seismograms from the regional 1D bedrock model at 5% damping. For the case of scenario 2, the calculated accelerograms at the bedrock in three components along cross sections I and II are shown in Figs. 12 and 14, respectively. While the plots of the response spectra ratio of the calculated accelerograms from scenario 2 along cross sections I and II are shown in Fig. 13 and Fig. 15, respectively.

Results show peak ground acceleration (PGA) of 39 cm/s^2 at epicentral distance of 31.7 km from the source in the transverse component at cross section I for scenario 1. For cross section II, a PGA of 70 cm/s^2 is obtained in the radial component at a distance of 30.3 km. Moreover, a PGA of 1259 cm/s^2 and 838 cm/s^2 are estimated in the radial component of cross section I and II at epicentral distances of 22.3 and 15.3 km from the source, respectively, for the case of scenario 2. As expected, the obtained PGA values from scenario 2 are larger than those from scenario 1, due to higher magnitude and shorter epicentral distance.

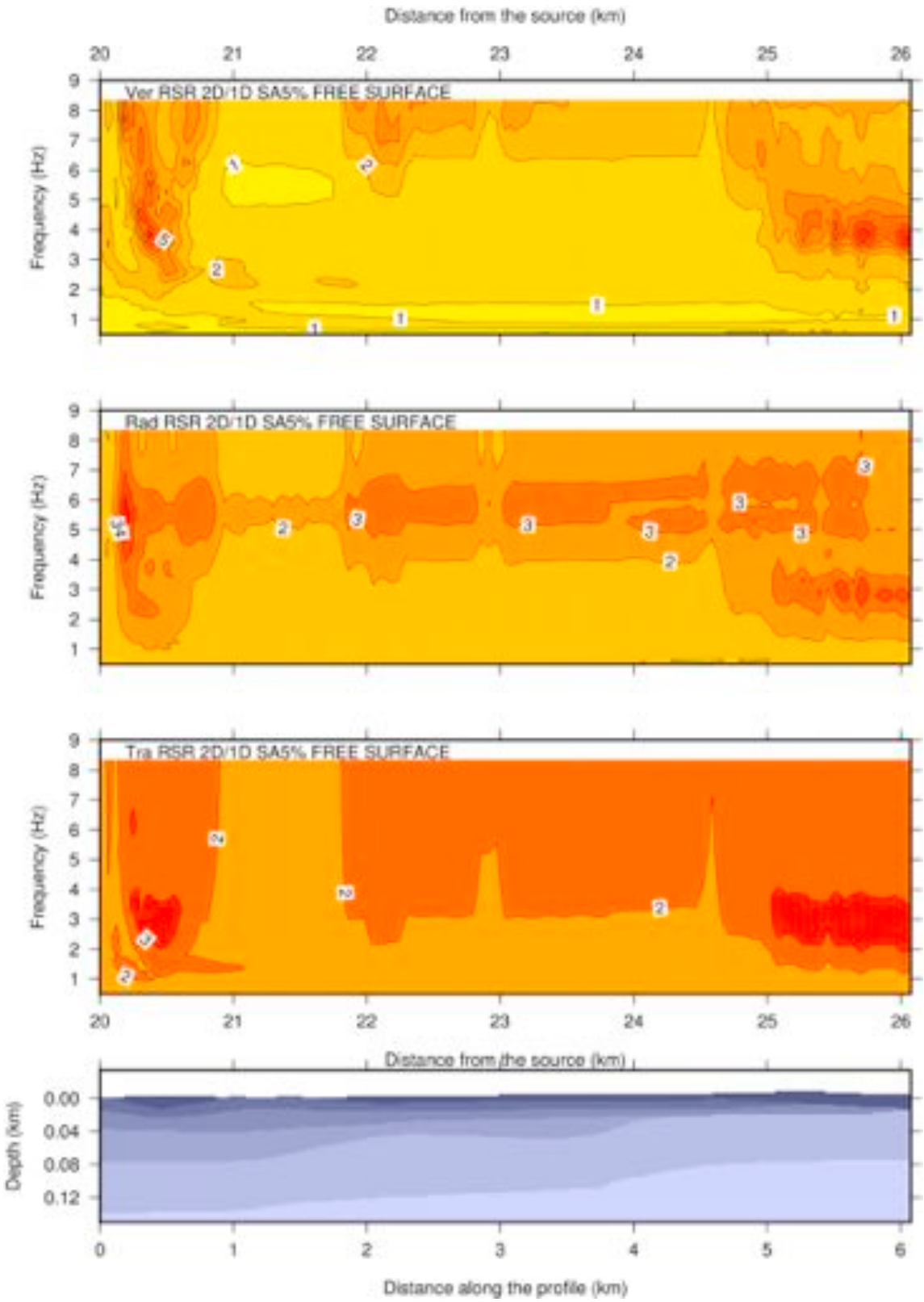

Fig. 13. Response spectra ratio (RSR 2D/1D) at 5% damping for the computed three-components synthetic accelerograms from scenario 2 along the cross section I.

The response spectra ratio plots in Figs. 9, 11, 13, and 15) clearly show high site amplification at the ground surface which reflects the geometry, local heterogeneity, and the subsurface topography of cross section I and II. From the RSR results of scenario 1, the maximum site amplification obtained along cross section I is about 4 in the vertical component at frequencies between 6 and 6.5 Hz at an epicentral distance of about 27 km from the source. In comparison, the maximum amplification along cross section II from the same scenario is about 4 and appears on the radial component at frequencies between 5 and 6 Hz and at a distance of 30 km from the source.

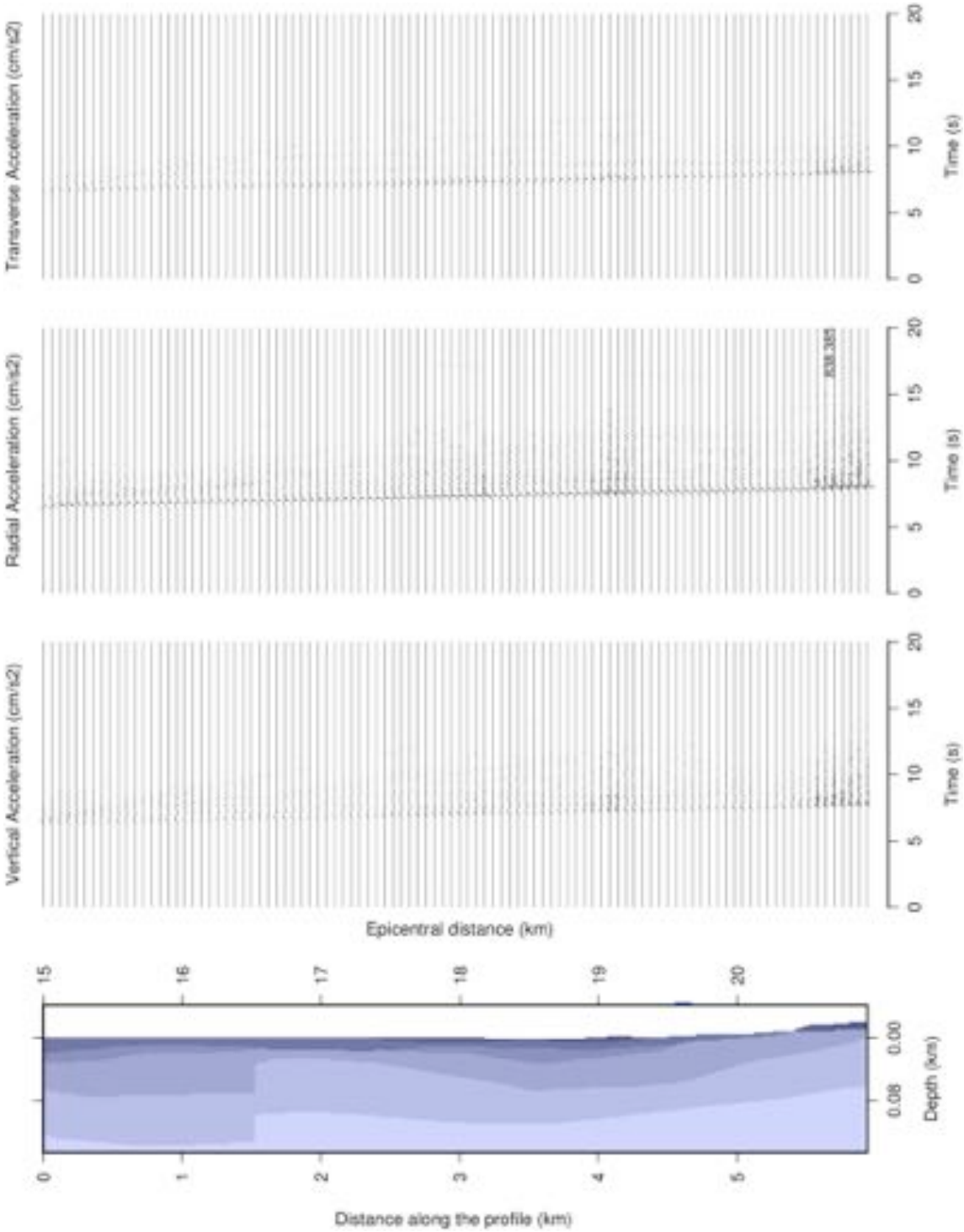

Fig. 14. Three components synthetic accelerograms at the ground surface for scenario 2 along the cross section II.

For scenario 2, the maximum amplification along cross section I is about 5 and is obtained on the vertical component at frequencies between 3.5 and 4.5 Hz at about 20.5 km from the source, while the maximum amplification from the same scenario in cross section II is about 3 at frequencies between 5 and 6.5 Hz for the radial component at a distance of 21 km from the source.

The discrepancy of RSR results in the case of scenario 1 and 2 for the same cross section could be a result of the change in earthquake size, propagation path, or the incident angle of wavefield. This reflects the fact that the site effects are not being persistent when an earthquake source changes (Molchan et al., 2011). This is especially significant in the Nile Delta and Valley, where the charactersistics of the sediments can have a large impact on the polarization in the horizontal plane (also defined amplification/de-amplification) of seismic waves and on ground failure or soil liquefaction (e.g. El-Sayed et al., 2004).

4.4. Ground motions modeling from scenario 3 (EW cross section III)

For the case of scenario 3 and cross section III, the calculated synthetic accelerograms at the ground surface and the RSR plots in the transverse, radial, and vertical components are shown in Fig. 16 and Fig. 17, respectively. A PGA of 571 cm/s^2 is observed in the radial

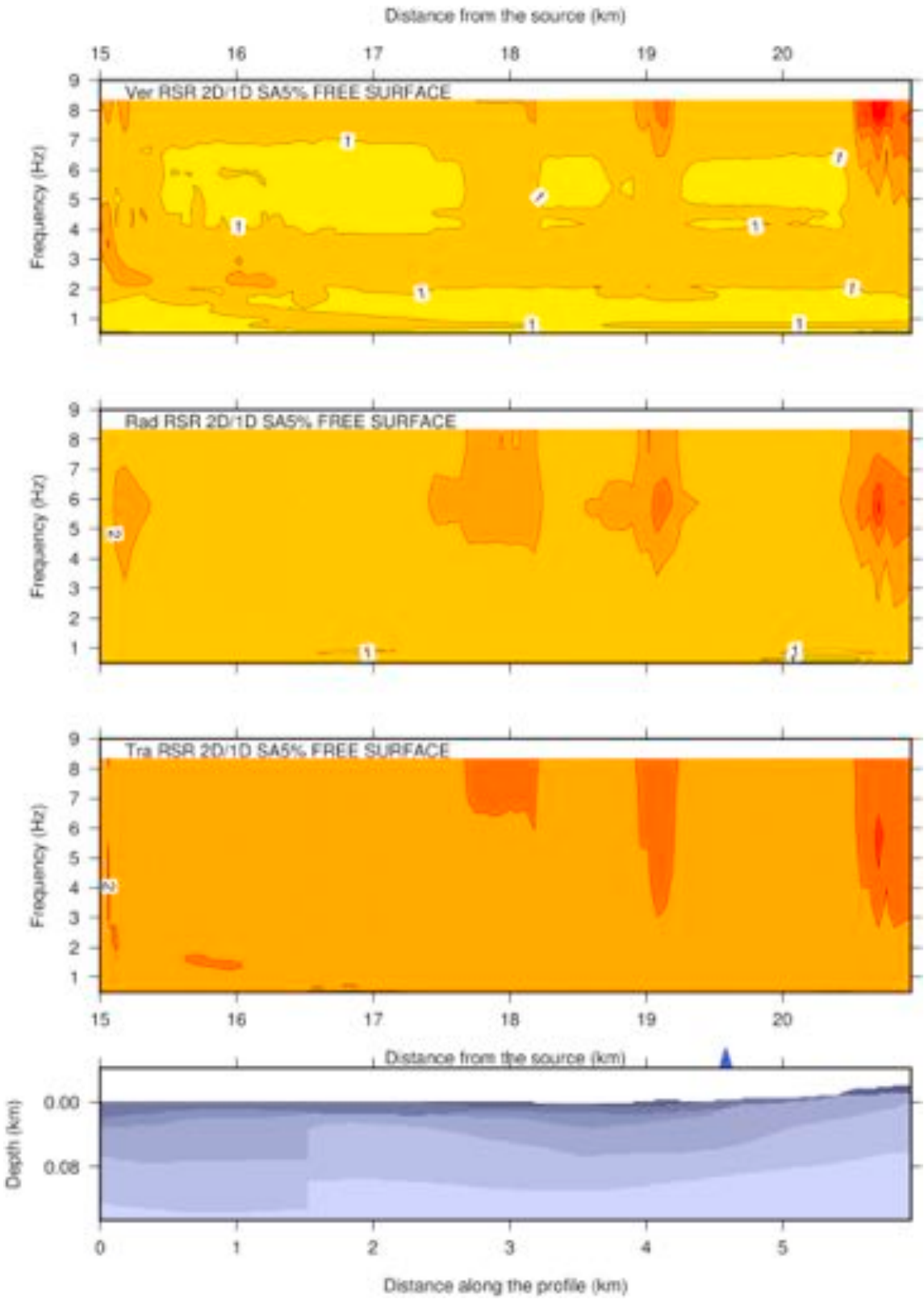

Fig. 15. Response spectra ratio (RSR 2D/1D) at 5% damping computed for the three-components synthetic accelerograms for scenario 2 along the cross section II. The blue triangle marks the location of the site for which the response spectra are provided. (For interpretation of the references to colour in this figure legend, the reader is referred to the web version of this article.)

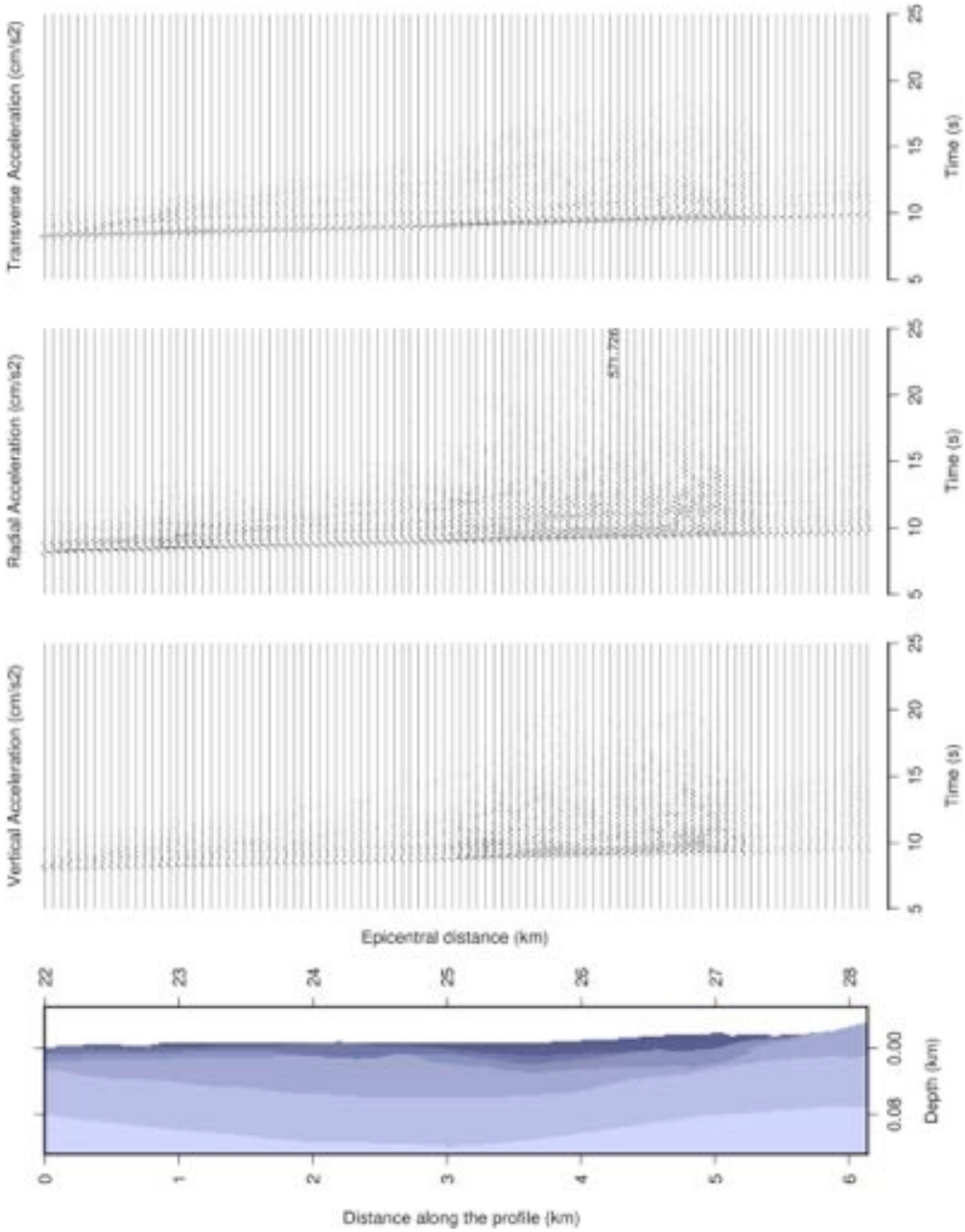

Fig. 16. Three components synthetic accelerograms at the ground surface for scenario 3 along the cross section III.

component at an epicentral distance of about 26.3 km from the source. The distribution of RSR values show that the maximum amplification is about 5 obtained for the vertical component at a frequency between 3.5 and 4 Hz, while the transverse and radial components show an amplification of about 3 in the frequency range from 2 to 4 Hz.

5. Site-specific multi-scenario seismic input

A multi-scenario site-specific seismic input taking into account the local site effect is needed for the seismic assessment of a selected cultural heritage building site located in historical Cairo. This is mainly due to the fact that different buildings can be affected more by different scenarios depending on their vibrational properties. As shown in Section 4, three earthquake scenarios and three cross sections have been considered to model the ground motion at the site of interest. These earthquake scenarios comprise one instrumental and two historical earthquakes. The calculations reported in Section 4 have been repeated many times in order to account for the stochastic nature of the seismic rupture process on the fault plane. In particular, for each considered source, 300 realizations of the rupture process are simulated; this number has been found to be suitable to stabilize the obtained variability in the response spectra accelerations (Fasan, 2017). From

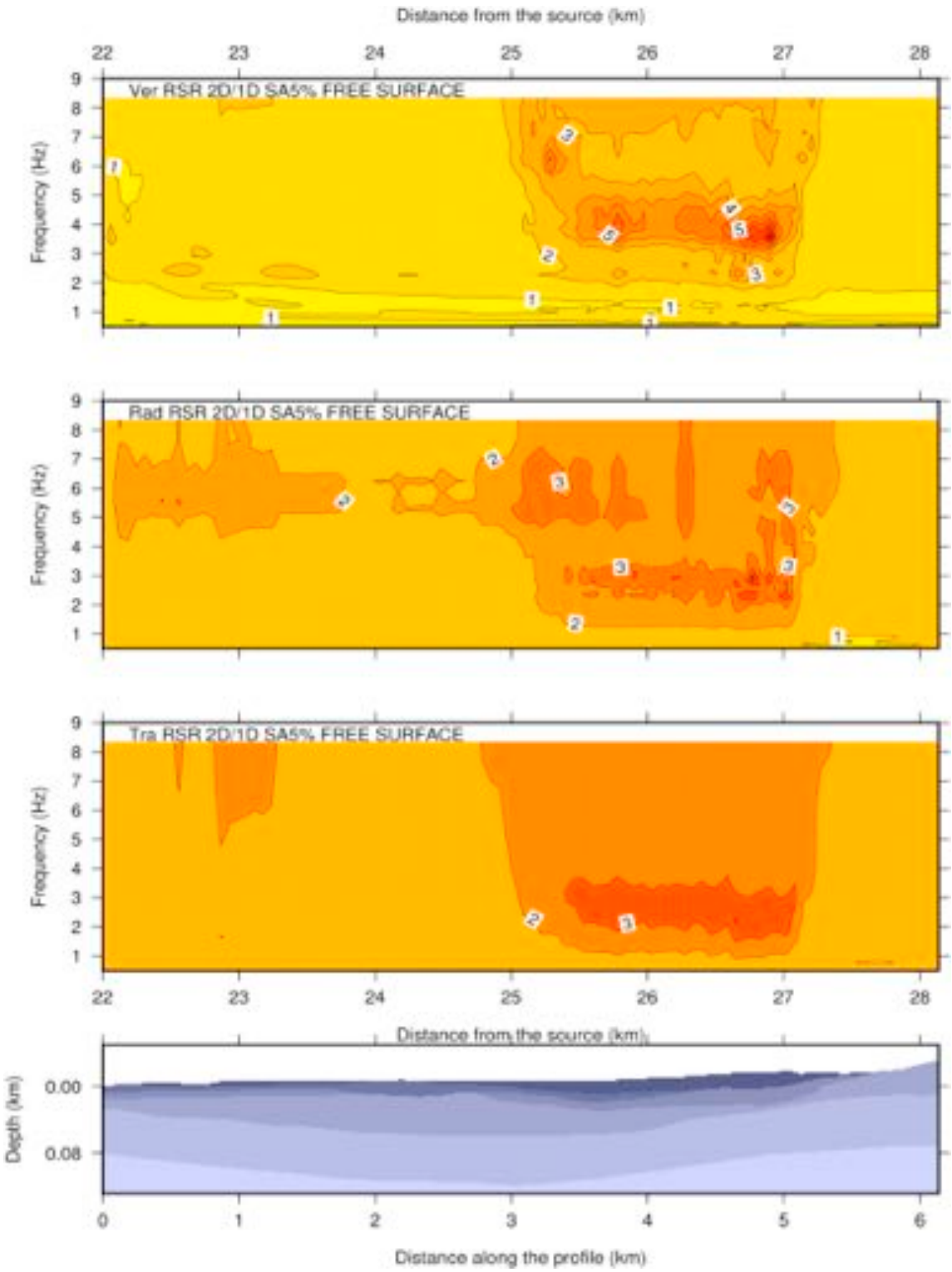

Fig. 17. Response spectra ratio (RSR 2D/1D) at 5% damping computed for the three-components synthetic accelerograms for scenario 3 along the cross section III.

each computed accelerogram the response spectrum is evaluated and the procedure presented in Fig. 4 is applied. Initially, the statistics of the computed spectral acceleration is done; the multi-scenario seismic input is then built retaining, at each vibrational period, the values of the scenario that show the highest median spectral acceleration. Fig. 18 shows this multi-scenario seismic input in the form of a response spectrum (5% damped). Variability of values from the median to the 95th percentile is reported and includes source, path and site effects.

It is worth noting that the procedure, as explained by Fasan (2017), allows also to select the accelerograms corresponding to a specific percentile of spectral accelerations. In fact, each computed response spectrum used to build Fig. 18 can be linked with its original simulated accelerograms. Therefore, when selecting accelerograms for non-linear time history analyses there is no need for filtering by magnitudes, distances, or site classifications, as done with real records extracted from a ground motion database. Moreover, there is no need for linearly

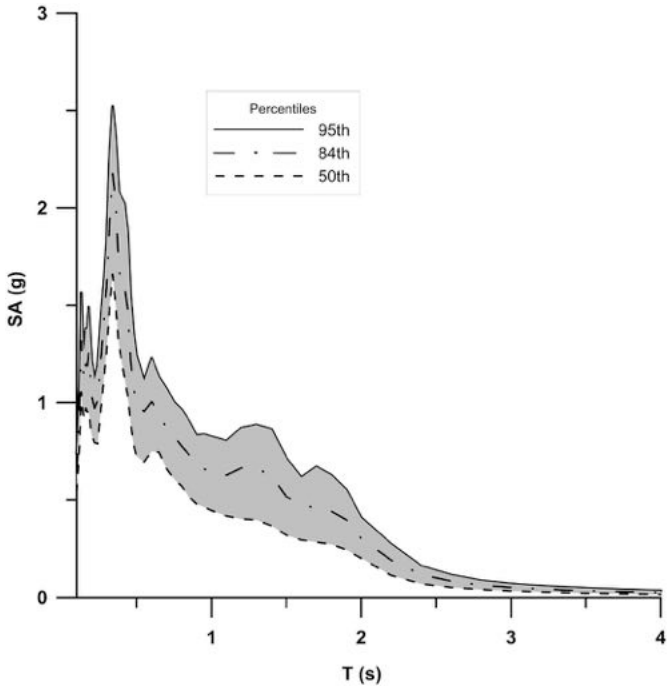

Fig. 18. Multi scenario response spectra (5% damping) at the selected site; the gray shaded area represents the SA range, between the 50th and 95th percentiles, controlled by the dominant scenario at the different periods.

scaling the accelerograms to match the target design spectra. Indeed, the accelerograms computed are all representative of the same site (site-specific) and scenarios. All accelerograms are three components, including the vertical one that can play a crucial role in the dynamic behavior of masonry structure as reported in Rinaldin et al. (2019).

6. Conclusions

This paper focuses on the seismic hazard assessment, including source, path, and potential local site effects, for the historical Cairo which contains a large number of cultural heritage buildings. Seismic hazard is evaluated through a detailed ground motion modeling using the modal summation and finite difference hybrid approach. The calculation of a multi-scenario site-specific seismic input in the form of response spectra at a site of a cultural heritage building is performed through a three-step analysis. The first step is a regional scale analysis to evaluate the ground motions at the bedrock level and identify the most hazardous scenarios. Subsequently, a site-specific analysis that accounts for source, path and local site effects is performed using the selected scenarios. Finally, results from the calculated scenarios are combined in a unique multi-scenario seismic input.

Three earthquake scenarios and three cross sections along the site of interest (2 NS and 1 EW) are used in the calculations, and synthetic physics-based accelerograms are computed along the selected profiles. A hybrid approach that combines both modal summation and finite difference techniques is used to model the propagation of the seismic waves from source to site of interest. Synthetic accelerograms are computed first in the a laterally non-varying 1D bedrock structural model with the MS. Then, they are introduced in a laterally heterogeneous 2D model of the cross sections and propagated using the FD approach. The calculation conducted in the 1D model represents ground motions at the bedrock level (i.e. without local site conditions). The response spectrum ratios between results of 2D and 1D models manifest the effect of the site subsurface topography of the adopted cross sections. Response spectrum ratios indicate that sites where there are steeper edges in the geometry subsurface profiles show higher amplifications. The maximum response spectral ratios for the site of interest range between 2 and 5 and they occur at frequency ranges between 1.0 and 7.0 Hz. After evaluating the amplifications, a site-specific multi-scenario seismic input at a site of a cultural heritage building is calculated considering the local site effect including the horizontal and vertical heterogeneities of the different cross section profiles. The chosen structure is the Madrasa (meaning school in Arabic) of the princess Tatar al-Higaziya. This structure was constructed in two stages. First, the mausoleum was built in 1348, as an extension to the princess Tatar's house, then after thirteen years the palace and the mausoleum were converted into the Madrasa (Williams, 2008).

According to the earthquake damage report of the Japanese Expert Team (1993), the one- and two-story adobe dwellings performed poorly during the earthquake and were the primary cause of the more than 500 earthquake fatalities. The occurrence of damage to low-rise buildings proves that the site amplification may happen at a higher frequency range which fit well with the obtained results of this work. High-rise structures, e.g. brick-firing kilns with masonry smokestacks approximately 20 to 30 m tall, are scattered throughout the Nile Valley but none was known to have toppled in the earthquake.

The results obtained in this work may represent an important step forward towards the proper seismic assessment under earthquake shaking, aiding in the preservation, and risk reduction for existing cultural heritage structures through both scientific and engineering knowledge. In this paper we have shown how to develop a database of accelerograms and response spectra for the definition of the seismic input at a specific site in historical Cairo. The same can be done for any other site in Cairo, and the outcome can be provided to potential stakeholders as a part of further study.

Funding

This work was partially supported by the Egyptian Ministry of Higher Education (Cultural Affairs and Missions Sector, Cairo) and by the (MAE-MHE) bilateral Egyptian-Italian project “Advanced seismic hazard assessment in the Nile Delta, including site effects from distant earthquakes”.

Declaration of Competing Interest

The authors declare that they have no known competing financial interests or personal relationships that could have appeared to influence the work reported in this paper.

Acknowledgements

The first author would like to thank Prof. G.F. Panza for the support obtained during the PhD studies. Constructive comments from the Editor: Prof. Vicki Moon and two anonymous Reviewers have greatly improved the manuscript. Last but not the least; the authors would like to thank Ms. Mesha Richard for revising the paper linguistically.

References

Ambraseys, N.N., 2001. Far-field effects of Eastern Mediterranean earthquakes in Lower Egypt. J. Seismol. 5 (2), 263–268.
Ambraseys, N.N., Melville, C.P., Adams, R.D., 2005. The seismicity of Egypt, Arabia and the Red Sea: a historical review. Cambridge University Press.
Behrens-Abouseif, D., 2000. The Cairo heritage: essays in honor of Laila Ali Ibrahim. AUC Press, Cairo.
CAPMAS (Central Agency for Public Mobilization and Statistics Arabic Republic of Egypt) report, 2017. Census of population, housing and establishments. Internal report.
Egyptian Geological Survey and Mining Authority “EGSMA”, 1981. Geologic map of Egypt 1:2000000. EGSMA.
El-Khrepy, S., 2008. Detailed study of the seismic waves velocity and attenuation models using local earthquakes in the northeastern part of Egypt. Ph.D. Thesis. Mansoura Univ, Egypt.
El-Sayed, A., Vaccari, F., Panza, G.F., 2004. The Nile valley of Egypt: a major active

graben that magnifies seismic waves. Pure Appl. Geophys. 161 (5), 983–1002.
Fäh, D., Iodice, C., Suhadolc, P., Panza, G.F., 1993. A new method for the realistic estimation of seismic ground motion in megacities: the case of Rome. Earthquake Spectra 9 (4), 643–668.
Fasan, M., 2017. Advanced seismological and engineering analysis for structural seismic design. University of Trieste, Italy.
Fasan, M., Magrin, A., Amadio, C., Romanelli, F., Vaccari, F., Panza, G.F., 2016. A seismological and engineering perspective on the 2016 Central Italy earthquakes. Int. J. Earthq. Impact Eng. 1, 395–420.
Gamal, M.A., 2009. Using microtremors for microseismic zonation in Cairo's crowded, urban areas. J. Seismol. 13 (1), 13–30.
Gorshkov, A.I., Hassan, H.M., Novikova, O.V., 2019. Seismogenic nodes (M≥ 5.0) in Northeast Egypt and implications for seismic hazard assessment. Pure Appl. Geophys. 176 (2), 593–610.
Gusev, A.A., 2011. Broadband kinematic stochastic simulation of an earthquake source: a refined procedure for application in seismic hazard studies. Pure Appl. Geophys. 168, 155–200.
Hassan, H.M., Romanelli, F., Panza, G.F., ElGabry, M.N., Magrin, A., 2017. Update and sensitivity analysis of the neo-deterministic seismic hazard assessment for Egypt. Eng. Geol. 218, 77–89.
Hussein, H.M., Elenean, K.A., Marzouk, I.A., Korrat, I.M., El-Nader, I.A., Ghazala, H., ElGabry, M.N., 2013. Present-day tectonic stress regime in Egypt and surrounding area based on inversion of earthquake focal mechanisms. J. Afr. Earth Sci. 81, 1–15.
Japanese Expert Team, 1993. Report of Japan Disaster Relief Team on the earthquake in Arab Republic of Egypt of October 12, 1992. pp. 77.
Kebeasy, T.R.M., Husebye, E.S., 2003. A finite-difference approach for simulating ground responses in sedimentary basins: quantitative modelling of the Nile Valley, Egypt. Geophys. J. Int. 154 (3), 913–924.
Kebeasy, R.M., Maamoun, M., 1981. Seismicity and earthquake risk of the proposed site of Shoubra al-Khaimah electric power station. Bull. Int'l Inst. Seismol. and Earthquake Energy 19, 21–33.
Lokmer, I., Herak, M., Panza, G.F., Vaccari, F., 2002. Amplification of strong ground motion in the city of Zagreb, Croatia, estimated by computation of synthetic seismograms. Soil Dyn. Earthq. Eng. 22 (2), 105–113.
Magrin, A., Gusev, A.A., Romanelli, F., Vaccari, F., Panza, G.F., 2016. Broadband NDSHA computations and earthquake ground motion observations for the Italian territory. Int. J. Earthq. Impact Eng. 1 (1–2), 131–158.
Mohamed, A.E.E.A., El-Hadidy, M., Deif, A., Elenean, K.A., 2012. Seismic hazard studies in Egypt. NRIAG J. Astron. Geophys. 1 (2), 119–140.
Molchan, G., Kronrod, T., Panza, G.F., 2011. Hot/cold spots in Italian macroseismic data. Pure Appl. Geophys. 168 (3–4), 739–752. https://doi.org/10.1007/s00024-010-0111-3.
Nunziata, C., Costa, G., Marrara, F., Panza, G.F., 2000. Validated estimation of response spectra for the 1980 Irpinia earthquake in the eastern area of Naples. Earthquake Spectra 16 (3), 643–660.
Panza, G.F., Romanelli, F., Vaccari, F., 2001. Seismic wave propagation in laterally heterogeneous anelastic media: theory and applications to seismic zonation. Adv. Geophys. 43, 1–95.
Panza, G.F., La Mura, C., Peresan, A., Romanelli, F., Vaccari, F., 2012. Seismic hazard scenarios as preventive tools for a disaster resilient society. Adv. Geophys. 53, 93–165.
Parvez, I.A., Vaccari, F., Panza, G.F., 2004. Site-specific microzonation study in Delhi metropolitan city by 2-D modelling of SH and P-SV waves. In: Seismic ground motion in large urban areas. Birkhäuser Basel, pp. 1165–1184.
Rinaldin, G., Fasan, M., Amadio, C., Noè, S., 2019. The influence of earthquake vertical component on the seismic response of masonry structures. Eng. Struct. 185, 184–193. https://doi.org/10.1016/j.engstruct.2019.01.138.
Romanelli, F., Vaccari, F., 1999. Site response estimation and ground motion spectrum scenario in the Catania area. J. Seismol. 3 (3), 311–326.
Said, R., 1975. "Subsurface geology of Cairo area," Memoire de L'Institue d'Egypte, Tome Soixante, Cairo. 70 pgs.
Said, R., 1981. The geologic evolution of the Nile river. Springer-Verlag, New York, NY 151 pg.
Said, R., 1990. The geology of Egypt. Brookfield, Netherlands.
Said, R., 2012. The geological evolution of the river Nile. Springer Science & Business Media.
Shata, A.A., 1988. Geology of Cairo, Egypt. Environ. Eng. Geosci. 25 (2), 149–183.
Slavov, S., Paskaleva, I., Vaccari, F., Kouteva, M., Panza, G.F., 2004. Deterministic earthquake scenarios for the city of Sofia. PAGEOPH 161 (N5/6), 1221–1237.
Sun, R., Vaccari, F., Marrara, F., Panza, G.F., 1998. The main features of the local geological conditions can explain the macroseismic intensity caused in Xiji-Langfu (Beijing) by the M s= 7.7 Tangshan 1976 earthquake. Pure Appl. Geophys. 152 (3), 507–521.
Sykora, D., Look, D., Croci, G., Karaesmen, E., 1993. Reconnaissance report of damage to historic monuments in Cairo, Egypt following the October 12, 1992 Dahshur earthquake. Army Engineer Waterways Experiment Station Vicksburg MS Geotechnical Lab. http://www.dtic.mil/dtic/tr/fulltext/u2/a325190.pdf.
Toni, M., 2012. Site Response ad seismic hazard assessment for the southern part of Cairo city, Egypt. In: Unpublished PhD thesis. Faculty of Science, Assiut University 151 pages.
Williams, C., 2008. Islamic monuments in Cairo: the practical guide. American Univ in Cairo Press.